AIAA AVIATION Forum
17-21 June 2019, Dallas, Texas
AIAA Aviation 2019 Forum

10.2514/6.2019-2887

Digital Twin Concept for Aircraft System Failure Detection and Correction

Omar Hazbon Alvarez[1] and Luis B. Gutierrez Zea[2]
Universidad Pontificia Bolivariana, School of Aeronautical Engineering, Medellin, Colombia.

Cees Bil[3]
RMIT University, School of Engineering, Melbourne, Australia.

Mario L. Fravolini[4]
University of Perugia, Department of Engineering, Perugia, Italy.

Marcello Napolitano[5]
West Virginia University, School of Mechanical and Aerospace Engineering, Morgantown, USA.

The air data system estimates vital flight parameters for correct and safe aircraft operation. One of the main components in this system is the Pitot tube sensor for measuring the total pressure and static pressure to estimate altitude, air speed, vertical speed and Mach number. The Pitot tube can supply incorrect measurement readings when its orifices are blocked by ice, dust or even insects. This paper describes the results of an ongoing research project to develop a solution to aircraft loss of control caused by an unreliable airspeed indication by incorporating the concept of an aircraft *digital twin*.

I. Nomenclature

$\boldsymbol{a}$	=accelerometer measurement
Ω	= angular velocity
$\dot{\Omega}$	= angular acceleration
$\boldsymbol{C}$	= direction cosine matrix
$\boldsymbol{V}$	= velocity
$\dot{\boldsymbol{V}}$	= acceleration
$\boldsymbol{r}$	= position
$\boldsymbol{q}$	= attitude quaternion
$\dot{\boldsymbol{q}}$	= attitude quaternion rate
$\boldsymbol{b}$	= instrument bias
$\boldsymbol{\alpha}$	= angle of attack
$\boldsymbol{\beta}$	= angle of sideslip
$\boldsymbol{F_t}$	= thrust force
$\boldsymbol{M_t}$	= thrust moment
$\boldsymbol{F_a}$	= aerodynamic force
$\boldsymbol{M_a}$	= aerodynamic moment
$\boldsymbol{m}$	= aircraft mass
$\boldsymbol{cg}$	= center of gravity
$\boldsymbol{I}$	= aircraft inertia
$\boldsymbol{BW}$	= bandwidth

Subscripts or Superscripts

$\boldsymbol{b}$	= body frame
$\boldsymbol{n}$	= navigation frame
$\boldsymbol{m}$	= measurement
$\boldsymbol{acc}$	= accelerometer
$\boldsymbol{gyro}$	= gyroscope

[1] Professor, School of Aeronautical Engineering, Universidad Pontificia Bolivariana, Medellin, Colombia, AIAA Senior Member.
[2] Professor, School of Aeronautical Engineering, Universidad Pontificia Bolivariana, Medellin, Colombia.
[3] Professor, School of Engineering, RMIT University, Melbourne, Australia, AIAA Associate Fellow.
[4] Associate Professor, Department of Engineering, University of Perugia, Perugia, Italy.
[5] Professor, School of Mechanical and Aerospace Engineering, West Virginia University, Morgantown, USA, AIAA Senior Member

II. Introduction

The Air Data System (ADS) plays a vital role in aircraft operation. The information provided by this device is used by the pilot and other aircraft subsystems for maneuvering and navigating within safe performance boundaries. Aircraft state parameters like pressure altitude, vertical speed, calibrated airspeed, Mach number, true airspeed, static air temperature, air density ratio, angle of attack and angle of sideslip are calculated by the Air Data Computer (ADC) from the information provided by the ADS Sensors. The basic air data sensors are the Pitot tube that provides information to the ADC about total pressure, the static port that provides information of the static pressure and the temperature probe that provides information of the total air temperature. For some applications, were the aircraft can reach angles of attack near the stall region or fly-by-wire flight control system applications, the ADS is provided with angle of attack and sideslip vanes.

There is a history of aircraft accidents caused by the failure of one of the ADS sensors: the Pitot tube. The most controversial accidents were AeroPerú flight 603 in October 1996 and Air France flight 447 in June 2009. In 2018 two accidents are suspected to be caused by the Pitot tube failure, Saratov Airlines flight 6W703 and Lion Air flight 610. Table 1 shows a list of some selected non-military aircraft accidents caused by Pitot tube failure since 1973 [1-15].

Table 1 Some non-military aircraft accidents caused by Pitot tube Failure or ADS sensors since 1973.

Date	Model	Aircraft Damage	Cause	Passengers and Crew	Casualties / Injured
January 30 1973	DC-9-21	Aircraft total Loss	Ice in Pitot tubes	33	0
December 01 1974	Boeing 727 - 251	Aircraft total Loss	Ice in Pitot tubes	3	3
July 28 1984	Learjet 25B	Aircraft total Loss	Pitot tube covers not removed	3	0
May 21 1986	Tupolev 154B-2	Aircraft total Loss	Ice on Pitot tubes	176	0
March 02 1994	MD-82	Structural damage	Ice on Pitot tubes	116	0
February 06 1996	Boeing 757 - 225	Aircraft total loss	Dust or insect debris blocking Pitot tubes orifices	189	189
October 02 1996	Boeing 757-23A	Aircraft total loss	Adhesive tape blocking ADS static port orifice	70	70
October 10 1997	DC-9-32	Aircraft total loss	Ice on Pitot tubes	74	74
April 7 1999	Boeing 737 4Q8	Aircraft total loss	Ice on Pitot tubes	6	6
October 17 1999	MD-11F	Aircraft total loss	Ice blocking Pitot tube drain orifices	2	0
June 3 2006	Dornier 328Jet-300	Aircraft total loss	Obstruction of Pitot tube orifices	8	0
June 01 2009	Airbus A330 - 202	Aircraft total loss	Obstruction of Pitot tube orifices	228	228
Feb 11 2018	Antonov 148	Aircraft total loss	Possible Ice on Pitot Tubes	71	71
Oct 29 2018	Boeing 737	Aircraft total loss	Possible ADS Failure	189	189

There are also cases were angle of attack vane failure caused aircraft accidents. This was the case for XL Airways flight 888T on November 2008 and it is also a presumed the cause for the Ethiopian Airways flight 302 accident on March 2019.

It has been observed that the Pitot-static system fails under certain atmospheric conditions of low temperature and high humidity. The sensor orifices or internal ducts are blocked with ice preventing actual pressure readings to be sensed by its transducer and as a result, the computed airspeed become erratic and unreliable. There are other possible causes of Pitot blockage like dirt, insects or even ground protection devices. The Pitot tube failure affects air safety as pilots may not be able to identify the failure and become confused due to unreliable and conflicting warnings. In unmanned air vehicles the situation is also critical because the autopilot is receiving erratic information from the ADS system causing a total loss of control.

To overcome the consequences of ADS sensor failures, aircraft manufacturers have implemented sensor redundancy with a voting scheme that detects and isolate faulty air data sensor signals, however under certain atmospheric circumstances all sensors fail at the same time and is known as common mode failure. Airbus equipped the A320, A330 and A340 with a Backup Speed Scale (BUSS) were a theoretical airspeed is estimated from pitch and thrust tables, however the system failed on Air France 447 [16]. The Airbus A350, a state of the art airliner, is using an extra air pressure information from the sensors of the engine nacelles that helps alleviating the effects of corrupted ADS sensor signals [17]. On the other hand, Boeing's approach to this problem was to equip the 787 Dreamliner with an airspeed estimation using information of angle of attack and inertial data called "Synthetic Air Speed", however this system failed on Jetstar flight JQ 07 [18].

The goal of this research is to develop an ADS tolerant to the Pitot-static sensor failure by means of a real time numerical estimation of the airspeed, using information from other airborne sensors and supported by a high-fidelity aircraft dynamic model called digital twin that will act as a virtual sensor. The digital twin concept is illustrated in Fig. 1.

Fig. 1 Aircraft digital twin concept.

III. Literature review

The airspeed sensor failure problem has been worked out by means of a Sensor failure detection identification and accommodation (SFDIA) task. SFDIA has been traditionally divided in two steps. The first step involves the detection of the sensor failure and identification (SFDI) of the sensor that is generating the unhealthy signal so the corrupted hardware can be isolated. Sensor failure accommodation (SFA), the second task, consist in the numerical estimation of the airspeed by means of a virtual sensor and the statistical comparison of this value with the sensor (or sensors) signal so the healthy parameter can be selected and used in the flight control system.

A. Sensor Failure and Identification

Napolitano et al [19] used three approaches for SFDI purposes based in statistical fault detection filters. The first approach analyses the sensor signal residual by means of a fixed failure detection threshold that uses a Cumulative Sum filter – CUSUM. The second approach tries to minimize the number of false detections or undetected corrupted signals by using adaptive signal residual thresholds and calling this algorithm the "floating limiter". The third approach is based on the analysis of the residual signals by using the statistical generalized likelihood ratio test method – GLRT. In either approach, the difference between the sensor measurement and the analytically estimated value, so called the residual, is compared with the computed threshold and the failure will be identified when the residual exceeds a particular threshold value thus triggering failure detection. Recent research efforts focus on giving robustness to the statistical fault detection algorithm to the previous approaches by using the exponentially weighted moving averaged – EWMA filter that can detect small shifts in the mean and standard deviation of the residual signals [20]. The EWMA filter tracks the EWMA mean of all previous samples so that the most recent are weighted more heavily than the older ones, preventing that the faults in previous time steps affect the current residual. These fault tolerant techniques can be extended to as many sensors as needed in conjunction with a bank of residual monitors to isolate the faulty sensor.

B. Model-Based Sensor Failure Accommodation

The model-based current airspeed estimation approaches take advantage of the well-known aircraft non-linear model [21, 22] and redundant measurements from the sensors onboard. The commonly used model state variables are the true airspeed, angle of attack, angle of sideslip, angular rates, Euler attitude angles and the aircraft position. The state control variables rely on the thrust force and the elevator, rudder and aileron deflections. The airspeed is implicit in all the twelve equations of the aircraft nonlinear model, however in Napolitano's early research it is stated that the airspeed is strongly correlated with the angle of attack equation and it suffices for the estimation of the airspeed. The researchers expressed this equation in a form that is suitable for parameter identification with a linear combination of unknown coefficients and known nonlinear functions of measured signals. The equation is evaluated at several instants on a time window to set up a linear system of equations that is solved for the unknown equation coefficients by means of least squares and taking advantage of previously recorded flight test data. The online estimates of the airspeed at a particular time are based on the online solution of the quadratic equation were the unknown coefficients are substituted by the LS estimate and only the positive value of the airspeed is selected.

C. Model-Independent Sensor Failure Accommodation

The model-independent virtual sensors are of great interest because the estimation method can be applied conveniently to any aircraft without information of the vehicle dynamics which most of the time is difficult to obtain. Researchers had tried several types of state estimators to predict the aircraft airspeed. The nonlinear behavior of the aircraft dynamics has caused the researchers to use Kalman filter based estimation methods in the form of Extended and Unscented Kalman filter. These estimation methods use information from the other airborne sensors to estimate the airspeed, particularly the three axis accelerations and angular rates from the IMU, roll and pitch angle measurements from the vertical gyro and angle of attack and sideslip from the ADS as stated by Napolitano et al [23].

A second type of model independent SFA methods tried by researchers in the aircraft airspeed estimation are based in flight test data correlations in the form of Neural Networks - NN. The NN is trained to learn the functional relationship between the airspeed and a set of correlated measurements provided by the other aircraft sensors. Different type of NN has been tested in simulation. Napolitano et al [24] and Turkmen et al [25], developed airspeed estimators using Multi-Layer Perceptron – MLP NN to take advantage of its flexibility for several applications, including function fitting and pattern recognition. The MLP is usually trained to learn the functional relationship between the airspeed and a set of correlated measurements provided by the other aircraft sensors. To reduce the real-time computational requirements of the MLP NN, Napolitano et al [24] used the Extended Minimal Resource Allocating Networks – EMRAN NNs that allows only the parameters of the most active neurons to be updated, while all the others are left unchanged. Some other types ANNs had been used in aircraft airspeed estimation. Husain [26] used a fully connected cascade ANN for estimation arguing that it requires lower computational effort that MLP and EMRAN ANNs.

The NN estimation methods described above require tailored time-consuming tuning procedures that usually produce unreliable performance when validated with actual flight data. To overcome this problem current research effort is being conducted by Balzano et al [27] based on a semiautomatic data driven approach to select model regressors and identify Nonlinear Autoregressive Exogenous – NARX input-output neural network prediction models. This approach provides online model adaption mechanisms to cope with time dependent and flight dependent levels of uncertainties. The drawback of the NARX estimation model is that being an autoregressive model, its prediction is influenced by the fault. Trying to unlink the estimation result from the fault the researcher's tried a feed-forward non-autoregressive MLP NN modelled which can provide a reliable multi-step ahead estimation independently of the occurrence of the fault.

D. Modelling Pitot tube faults

The fault on the airspeed sensor is usually modeled by different authors like in Napolitano [23] as an additive bias. Two suddenly fault scenarios commonly used in fault detection and identification practice are usually implemented: a sudden bias (SB) failure and a slow ramp bias (SRB) failure as shown in Fig. 2 and Fig. 3 respectively as shown in Ref. [28]. The residual signal used for SFD is defined as the difference between the measured airspeed from the ADS and the estimated airspeed as shown in Fig. 4 and published in Ref. [28].

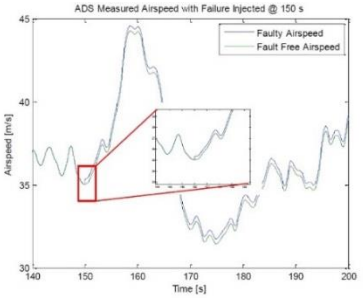

Fig. 2 SB failure.

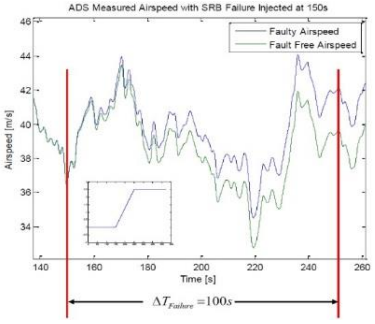

Fig. 3 SRB failure.

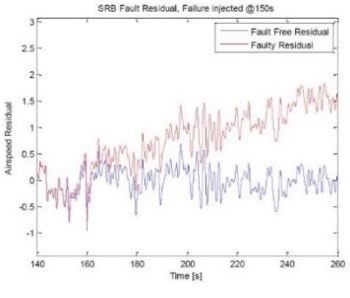

Fig. 4 Residual signal.

Theoretically the residual signal should approach to zero in the fault free condition scenario, but in the real world, due to modelling uncertainties and noise, the residual signal is different from zero. It is found in experiments that the raw residual signal has a significant autocorrelated length that is introduced mainly by uncertainties in the low frequency range. Since statistical detectors perform optimally when residual signals are completely uncorrelated, a whitening filter is usually designed to remove the residual signal correlation.

IV. Proposed Methodology

The objective of the project is to develop a new approach to perform SFDIA in case of ADS sensor failure. The SFDIA algorithm estimates the aircraft airspeed and other aircraft parameters using information from gyroscopes and accelerometers. A Global Positioning System - GPS, a magnetometer and a barometric altimeter are used as aiding sensors for estimation purposes. The sensor data fusion and estimation are done by a Kalman Filter based algorithm with the help of an accurate aircraft dynamic model acting as a virtual sensor referred to as the *"Aircraft Digital Twin"*. FDI will be carried out automatically by statistical evaluation of the sensor residual signal and accommodation will be done automatically by modulating the faulty sensors covariance, giving less weight during the estimation process. The proposed system concept is shown in Fig. 5.

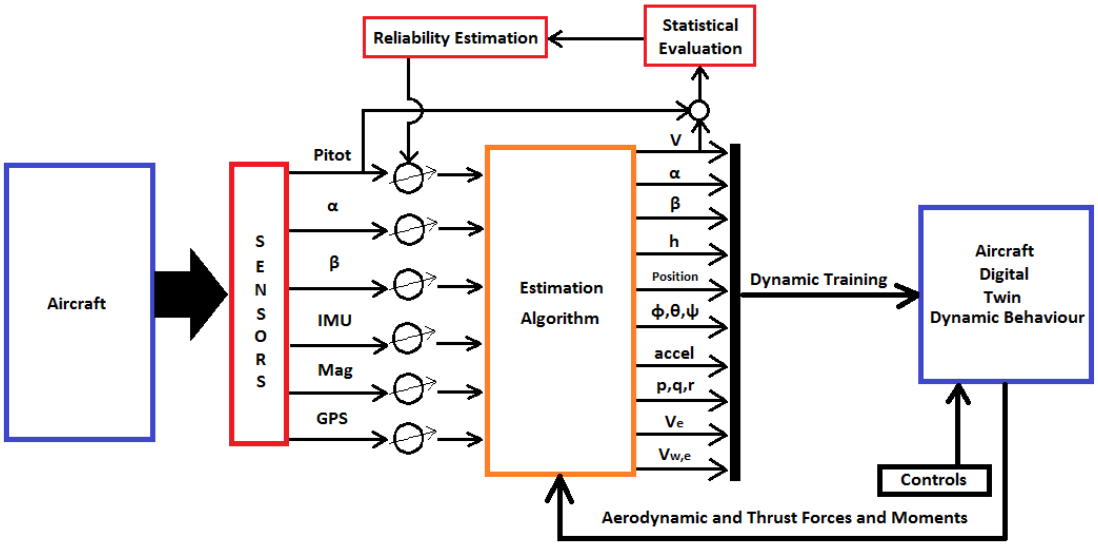

Fig. 5 Proposed airspeed estimation scheme.

A. Simulation Tools

The development of the estimator requires an aircraft flight simulation that provides information of the aircraft state to the sensor models and two approaches are being used. The first simulation approach is used for development purposes and consist in a Simulink® model of a Ryan Navion aircraft constructed from geometric, aerodynamic and propulsion data published by Seckel [29] and featuring an automatic flight control to generate cruise, turn and climb maneuvers during a 200 second flight time. The second simulation approach consist in an XPlane-11 based flight simulation that communicates in real time via UDP port with the estimation algorithm in Simulink and it will allow to use a human pilot to test the estimation algorithm at RMIT's FlyThisSIM Touch Trainer© flight simulator.

B. Sensor Simulink Models

The aircraft flight simulation provides true state data to the sensor models: latitude, longitude, altitude, velocity, angular velocity, linear accelerations, dynamic pressure, angle of attack, angle of sideslip, static pressure and static temperature. Sensor models will add noise, bias and dynamics to the true aircraft state variable signals so its behavior mimics the actual sensors. The following instruments were used:

- Xsens MTi G 700 Series sensor suit which contains an IMU (Gyroscopes and Accelerometers), GPS and a Magnetometer.
- Aeroprobe Micro Air Data System V2.0 wich contains the Pitot-static probe, and provides measurements of angle of attack and angle of Sideslip. This instrument come with an air data computer.

- Honeywell Linear Position Transducers are used to read the position of Flaps, Ailerons, Elevator, Rudder and Throttle.

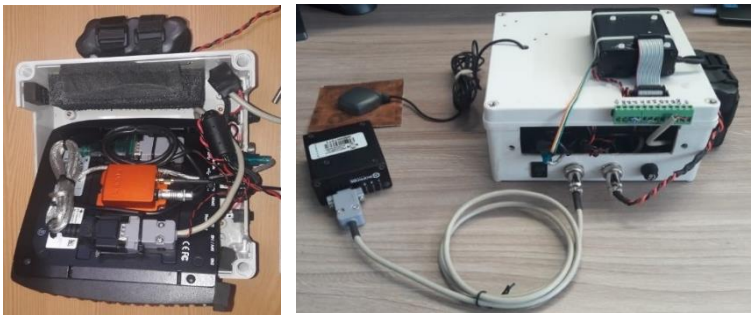

Fig. 6 Instrumentation for real-time inflight state estimation.

The sensor signals are processed in Fit PC - IPC2 computer with an Intel core i7 processor, solid state disk of 512GB, 16 GB RAM. Fig. 6 shows the developed instrumentation suite. The instrument signals were registered during a period of 20 minutes to compute its statistics as shown in table 2.

Table 2 Sensor Data.

Instrument	Sensor		Bias	Bias Standard Deviation	Noise Standard Deviation	Bandwidth [rad/s]	Sample Time [s]
ADS	Pitot		0	-	0.1	2*pi*100	0.02
	Alpha Vane		0	-	0.0001	2*pi*10	
	Beta Vane		0	-			
	Barometric Altimeter		0	-	0.1	2*pi*10	
	Thermocouple		0	-	0.1	2*pi*0.1	
IMU	Accelerometer		0	X: 0.0000166278915096521	X: 0.0166278915096521	2*pi*40	0.01
				Y: 0.0000210908739381218	Y: 0.0210908739381218		
				Z: 0.000098348406709339	Z: 0.0098348406709339		
	Gyroscope		0	X: 0.00000144095816668194	X: 0.00144095816668194		
				Y: 0.0000015453608741964	Y: 0.0015453608741964		
				Z: 0.00000158938163186551	Z: 0.00158938163186551		
Aiding Sensors	Magnetometer		0	Latitude: 0	Latitude: 0.0041428199321538	2*Pi*40	0.02
			0	Longitude: 0	Longitude: 0.0069532526571309		
			0	Altitude: 0	Altitude: 0.00947124844151009		
	GPS	Position	0	Horizontal: 6.45060790039193e-11	-	-	0.25
			0	Vertical: 0.000764384712305632			
		Speed	0	Horizontal: 0.0419758512436594			
			0	Vertical: 0.0194447270856484			

The sensor dynamics was modelled as a first order model in state space form as shown in Fig. 7. For each sensor signal component "i", the state space dynamic model was written as:

$$\dot{x}_i = Ax_i + B\,u_i \quad (1)$$
$$y = C\,x_i + D\,u_i \quad (2)$$

Where:

$$A = \begin{bmatrix} -BW & 0 & 0 \\ 0 & -BW & 0 \\ 0 & 0 & -BW \end{bmatrix}, B = \begin{bmatrix} BW & 0 & 0 \\ 0 & BW & 0 \\ 0 & 0 & BW \end{bmatrix}, C = \begin{bmatrix} 1 & 0 & 0 \\ 0 & 1 & 0 \\ 0 & 0 & 1 \end{bmatrix}, D = \begin{bmatrix} 0 & 0 & 0 \\ 0 & 0 & 0 \\ 0 & 0 & 0 \end{bmatrix}$$

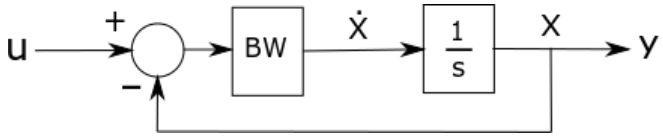

Fig. 7 Sensor dynamics in state space form.

C. Air Data System

The ADS models use the dynamic pressure, angle of attack, angle of sideslip, atmospheric pressure and temperature as input signals and it will add noise and bias were necessary in each sensor model to return the measured values of the dynamic pressure, angle of attack, and angle of sideslip, atmospheric pressure and atmospheric temperature. Figure 8 shows the Simulink block diagram of the ADS.

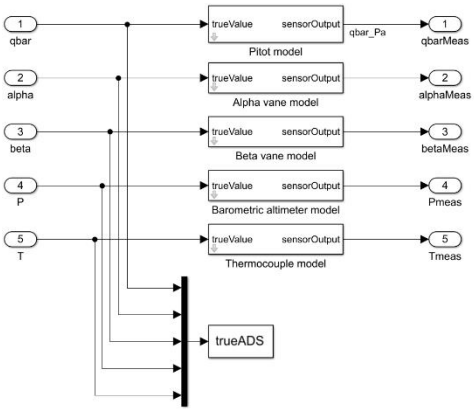

Fig. 8 Simulink model of Air Data System.

The Pitot was modelled using as input signal the dynamic pressure trough a zero-order hold to convert the continuous signal to discrete time. The sensor dynamics was modelled using the discrete state space model to which a white noise and a bias modelled as a random walk was added to obtain the dynamic pressure measured signal. Fig. 9 shows the Simulink block diagram for this sensor.

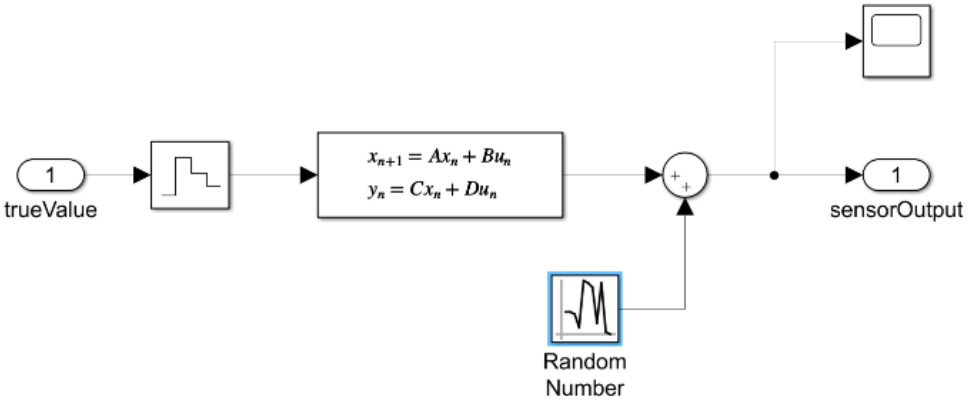

Fig. 9 Simulink model of the Pitot sensor.

The angle of attack vane sensor was modelled using as input signal the angle of attack to which a white noise and a bias modelled as a random walk is added. The sensor dynamics is modelled as a first order state space model. The signal enters a zero-order hold so a conversion from continuous system to discrete time is carried out before giving as output the measured angle of attack. A similar model is applied to the sideslip angle vane, the barometric altimeter and the temperature probe sensors but using as inputs signals the sideslip angle, the ambient static pressure and the ambient air temperature respectively. Fig. 10 shows the Simulink block diagram for these sensors.

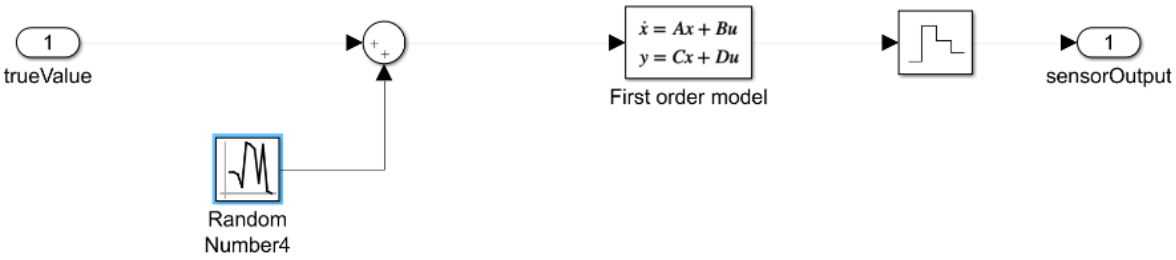

Fig. 10 Simulink model of the angle of attack, sideslip, barometric altimeter and temperature sensors.

D. Inertial Measurement Unit (IMU)

The IMU is composed of a 3-axis accelerometers and gyroscopes with angular velocity and linear acceleration as inputs respectively. To each signal a white noise and a bias is added, modelled as a random walk. The noisy and biased signal of each sensor is subjected to a first-order model dynamics in state space form and a zero-order hold to convert the continuous time signal to discrete time before it outputs the measured acceleration and angular velocity. True accelerometer and gyroscope bias signals are taken directly from the random walk. Figures 11 and 12 show the IMU Simulink© block diagram and each sensor model respectively.

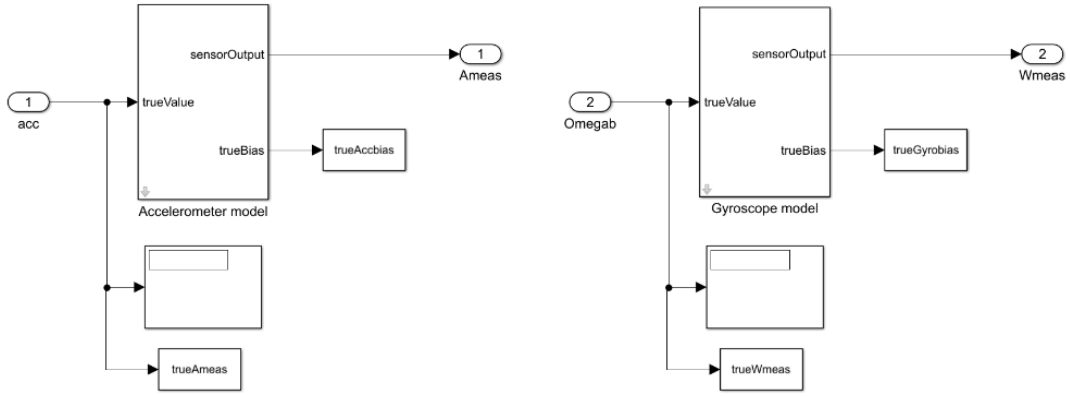

Fig. 11 IMU Simulink model.

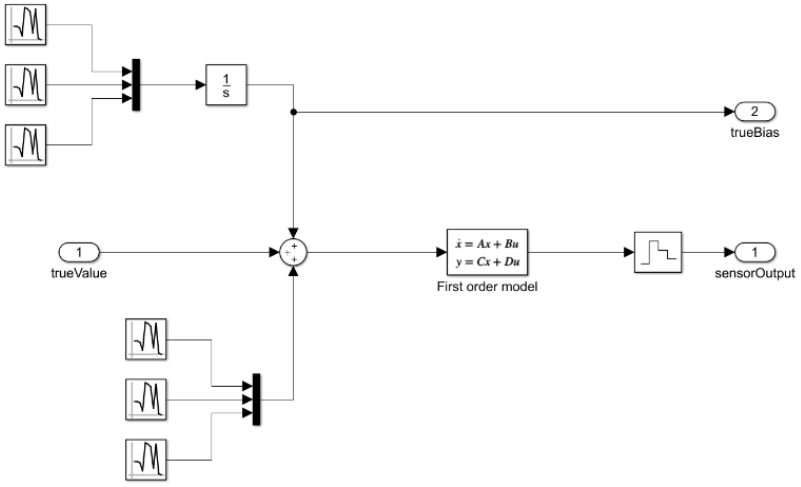

Fig. 12 Accelerometers and Gyroscopes Simulink model.

E. Magnetometer

The magnetometer was modelled using latitude, longitude, altitude and C_b^e as inputs and returning the Earth's magnetic field vector in the aircraft position and its true bias b_m. The Simulink model was constructed using a Matlab embedded function block that runs the *wrldmagm* function. White noise and a bias modelled as random walks are added to the *wrldmagm* output signal. Finally, the noisy and biased signal passes thru a first order state space model to mimic its dynamics and a zero-order hold to convert from continuous to discrete time. Figure 13 and Fig. 14 shows the magnetometer Simulink© block diagram with the embedded Matlab function and the sensor model respectively.

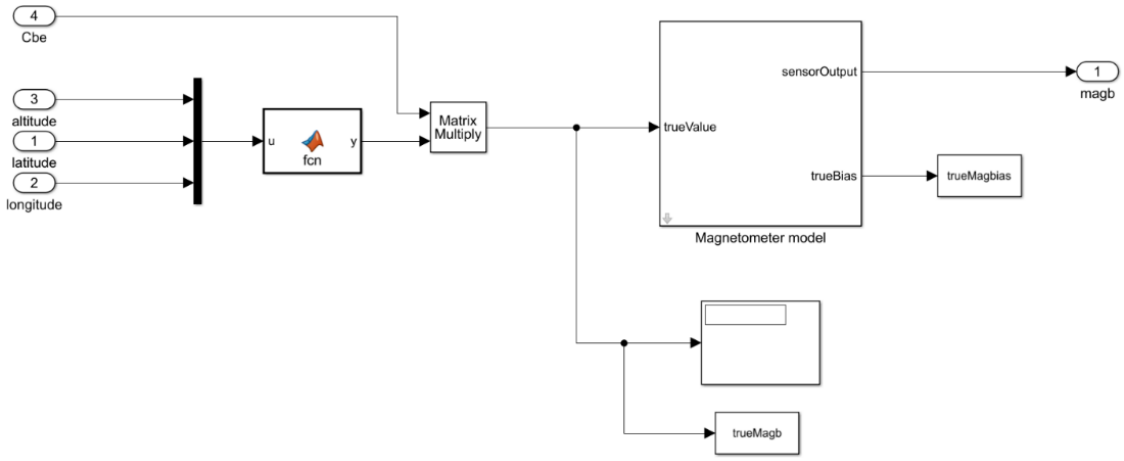

Fig. 13 Magnetometer Simulink model – World Magnetic Model embedded function.

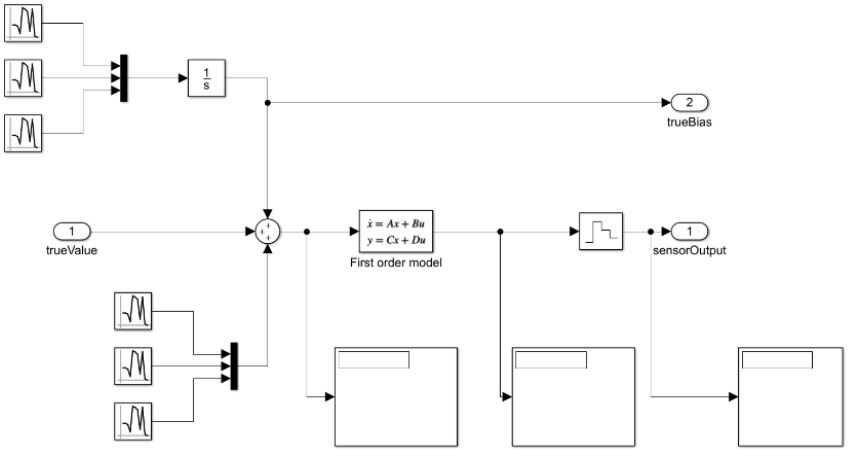

Fig. 14 Magnetometer Simulink model.

F. Global Positioning System (GPS)

The GPS model takes the simulation values of latitude, longitude, altitude and velocity as inputs. A bias modelled as a random walk that passes through an integrator is added to each position component. A zero-order hold and a unit delay is applied to the biased signal before the output of the GPS measured position. Figures 15 and 16 show the GPS position Simulink© block diagram and its sensor model respectively.

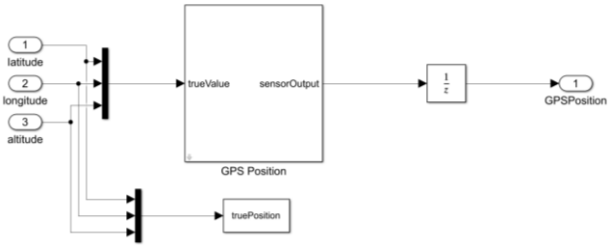

Fig. 15 GPS Simulink model (position).

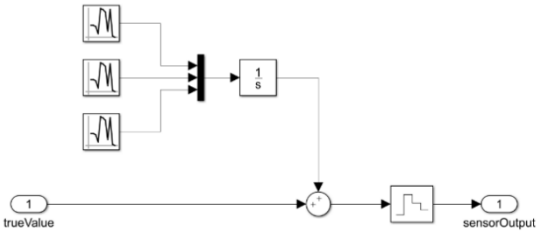

Fig. 16 GPS Simulink model (position).

The GPS velocity is modelled by adding a bias to each component of the simulation velocity. Then the biased velocity signal is passes through a zero-order hold and a unit delay before giving the GPS measured velocity as output. Figures 17 and 18 show the GPS velocity Simulink© block diagram and its sensor model respectively.

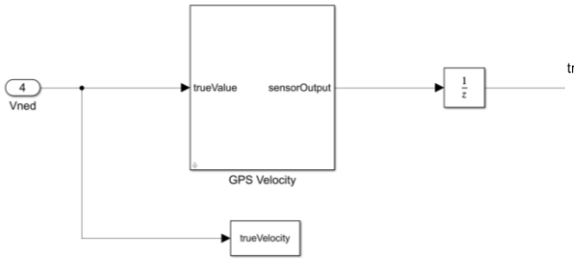

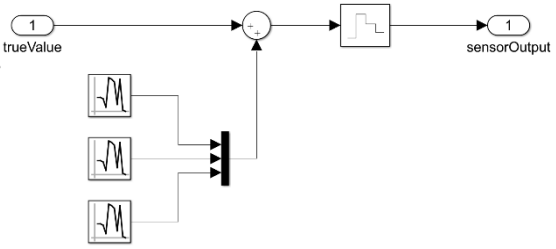

Fig. 17 GPS Simulink model (velocity). **Fig. 18 GPS Simulink model (velocity).**

V. Navigation System Extended Kalman Filter

The navigation system fuses sensor information from the IMU (gyroscopes and accelerometers), global positioning system GPS, a 3-axis magnetometer and a barometric altimeter in a framework of Extended Kalman Filter with sequential measurement update (SMU-EKF). In this estimation method, the sensor measurements can be easily fused together regardless of the number of sensors, sensor update rates, and sensor data dimensions as stated and well documented by Oh and Johnson [30].

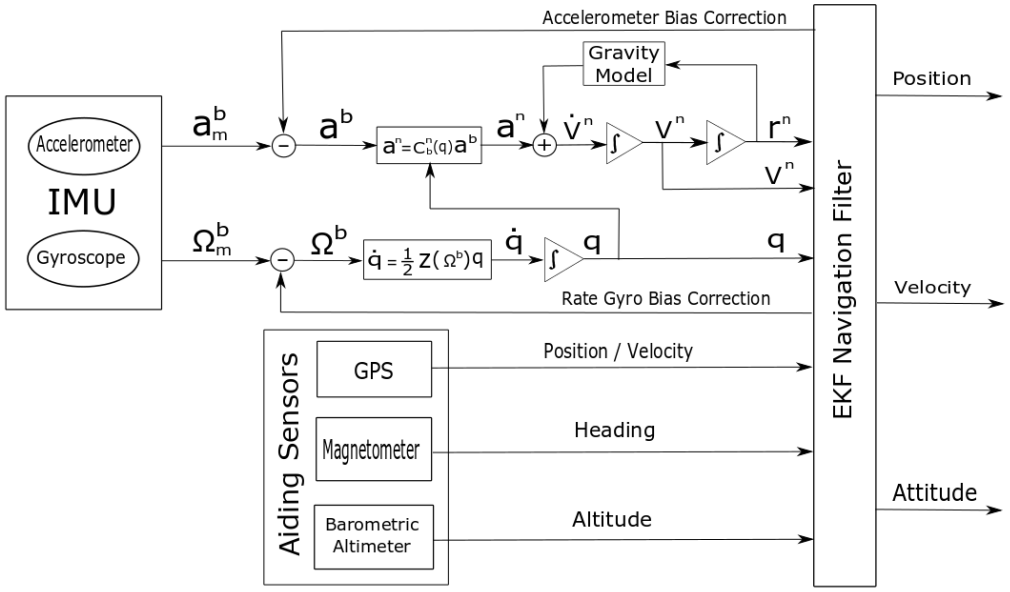

Fig. 19 Navigation System Extended Kalman Filter.

The core sensor in the estimation algorithm is the IMU, however to increase the accuracy of the estimation a GPS, a 3-axis magnetometer and a barometric altimeter are used as aiding sensors. The filter´s estimated state includes the aircraft position, velocity, attitude, accelerometer bias and gyroscope bias. The IMU provides information of the measured linear acceleration a_m^b and measured angular velocity Ω_m^b. The navigation EKF algorithm estimates the IMU sensor bias to correct each measured signal and obtain the unbiased aircraft's linear acceleration a^b and angular velocity Ω^b. The aircraft's acceleration has to be transformed from the body axis to the navigation frame using the direction cosine matrix C_b^n to obtain a^n. Since a^n is a specific force, gravity must be added to obtain the aircraft acceleration in the navigation frame $\dot{V}^n$. By integrating twice, the aircraft speed $V^n$and position r^n in the navigation frame are obtained. As shown in fig. 19, r^n is used in conjunction with the world gravitation model to compute the gravity vector. The aircraft attitude q is obtained by integration of the attitude rate $\dot{q}$ which is computed when the angular velocity Ω^b feeds the quaternion kinematical equations.

Figure 20 shows the aircraft velocity estimation results. The aircraft start flying to the north and at 20 second flight time the aircraft turns to the east 45 degrees and continue level flight. At 120 seconds of flight time the aircraft start climbing until 180 seconds of flight time where it levels and start cruise flight. The estimated velocity follows the true velocity accurately during all aircraft maneuvers. The estimated downward component of the aircraft velocity deviates in one m/s during climb, in the rest maneuvers the airspeed components deviate in 0.15 m/s.

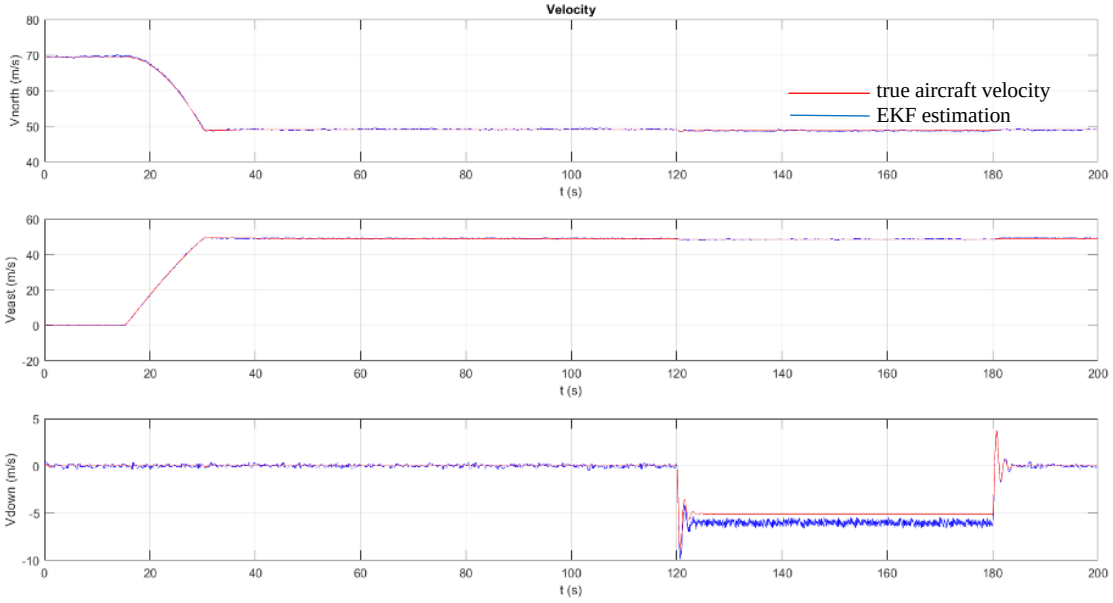

Fig. 20 Aircraft velocity estimation.

Figure 21 shows the aircraft attitude estimation. The estimation accurately follows the aircraft attitude true value in all maneuvers, particularly in roll and yaw. The pitch estimation accurately follows the true value. At the beginning of the climb there is a deviation from the estimation of one degree and at the end of the climb when the aircraft is leveling for cruise there is a deviation of two degrees, however in both cases the estimation in pitch converges to the true value in 20 seconds.

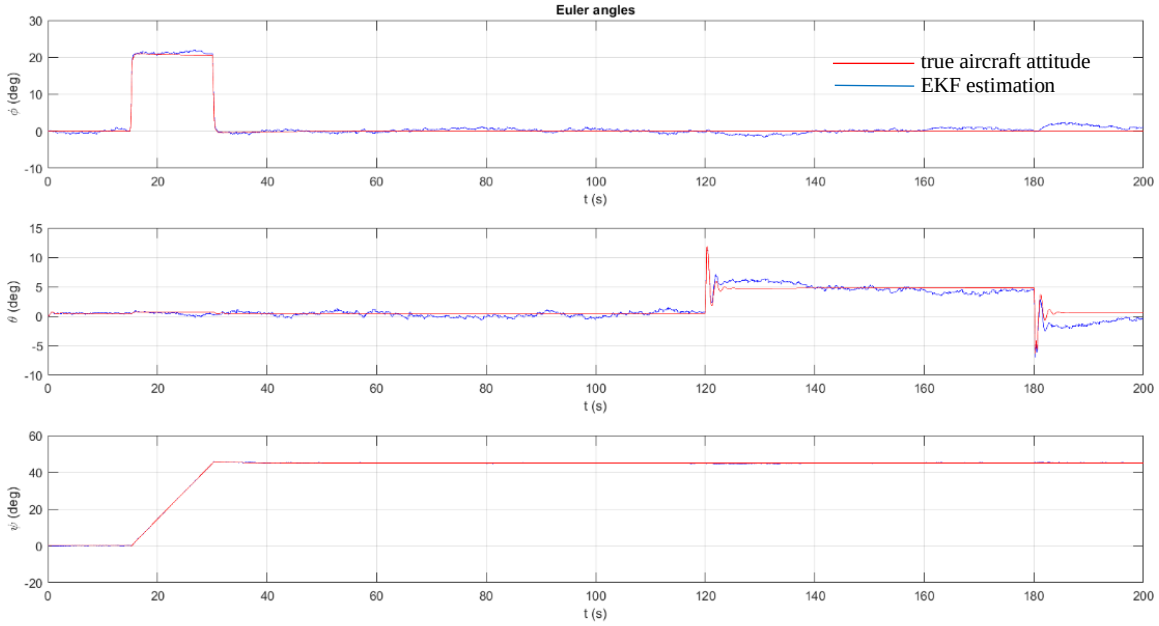

Fig. 21 Aircraft attitude estimation.

Figure 22 shows the aircraft position estimation. The estimated altitude at the beginning of the flight reaches a deviation of 100 meters from the true altitude value. The estimated altitude starts to converge at 40 seconds of flight and it reaches a good accuracy during the climb. This behavior can be caused by the low sampling time of the GPS used. A second reason is that this simulation was performed without including the barometric altimeter as an aiding sensor. In contrast the latitude and longitude estimation is very accurate, the deviations are in the order of 10^{-3}degrees.

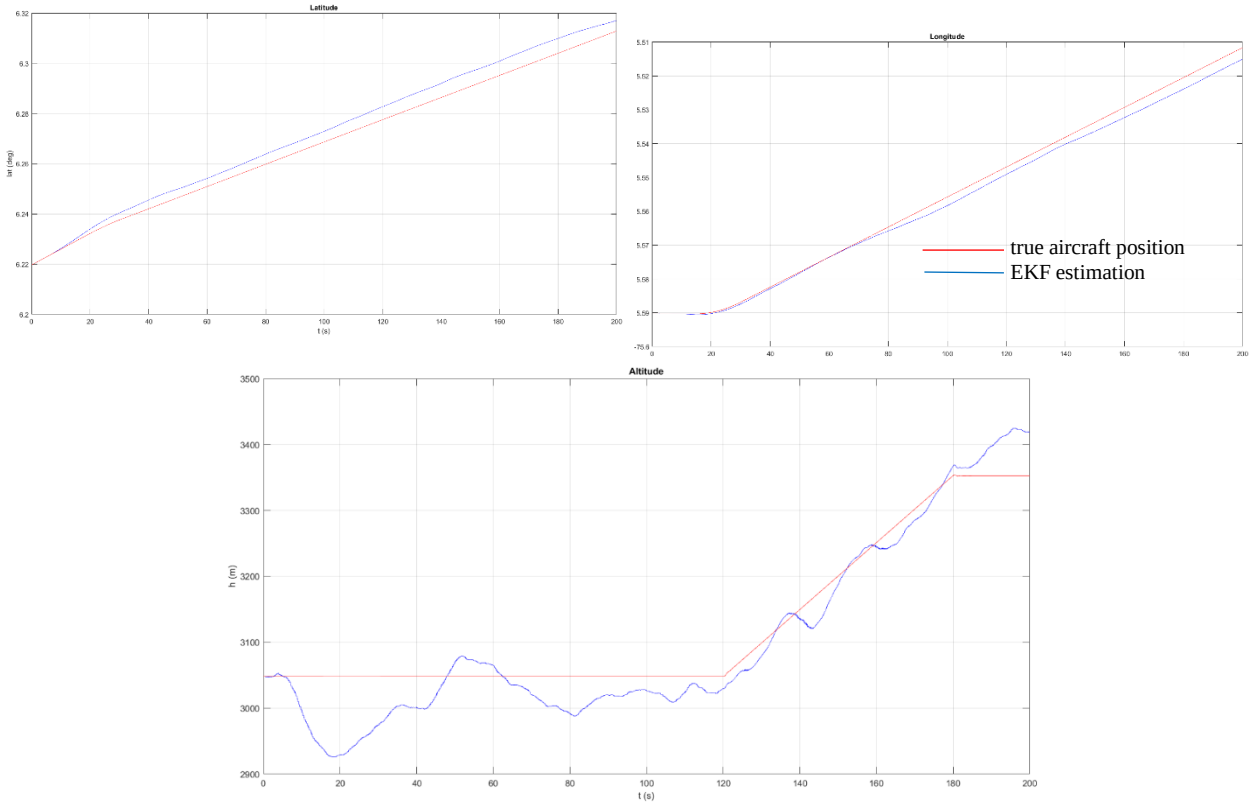

Fig. 22 Aircraft position estimation – Latitude, Longitude, and Altitude.

This simulation was repeated three times by varying the sensors bias and noise parameters without noticing an effect on the estimation accuracy.

VI. Current research on EKF navigation filter

The estimation results described in the previous section were computed without the implementation of the aircraft digital twin. Current research efforts are focused on the integration of the aircraft digital twin with the estimation algorithm described above. Figure 23 shows the integrated navigation system with the aircraft digital twin.

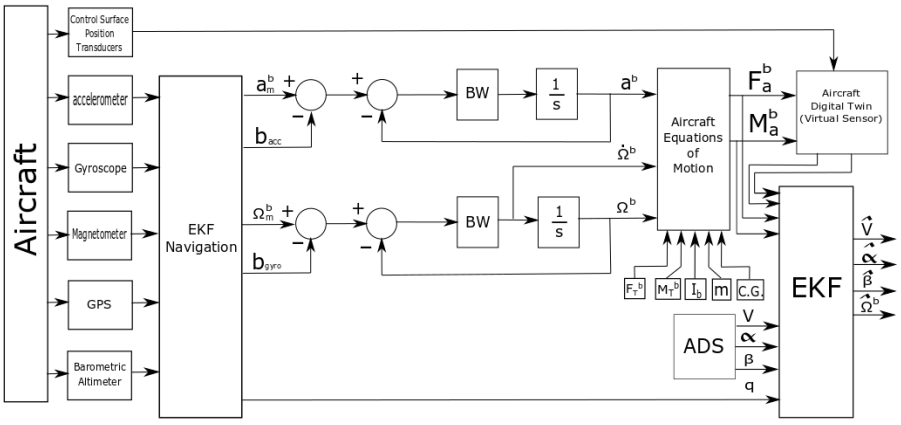

Fig. 23 Proposed estimation filter.

The estimation algorithm described in previous section provide accurate information of a^b and Ω^b. This values will pass through a first-order filter to simulate its dynamics. In the case of $\Omega^b$the value of its derivative $\dot{\Omega}^b$can be extracted. These values can be used together with the propulsion force F_t^b and moment M_t^b, the aircraft's controls, inertia matrix I_b, mass m and CG location to feed the equations of motion (3) and (4) to obtain the measured aircraft's aerodynamic force F_a^b and moment M_a^b.

$$M_a^b = I_b\dot{\Omega}_b - M_t^b + \Omega_b \times I_b \times \Omega_b \tag{3}$$

$$F_a^b = ma^b - F_t^b \tag{4}$$

The values of F_a^b and M_a^b will be used for two tasks. The first task will be to feed a second Kalman based estimation algorithm in conjunction with the attitude estimated in the navigation EKF filter and the measured values of airspeed, angle of attack and sideslip from the ADS. The second task will be to train the aircraft digital twin model that will act as a virtual sensor and that it will also provide virtual values of F_a^b and M_a^b to the second EKF, aiding in the estimation of the airspeed, angle of attack, angle of sideslip and w^b in the case of an ADS failure.

VI. Conclusion

This paper discusses different methods to estimate the aircraft airspeed and other state variables in case of a Pitot tube failure. The EKF navigation filter with sequential measurement update has shown to be a promising tool in the estimation of the airspeed, attitude and position with enough accuracy and low computational effort. The addition of adding sensors like the barometric altimeter to the estimation and the digital twin virtual sensor will increase the accuracy of the estimation filter especially in the estimation of the downward component of the velocity and the altitude. Higher GPS sample rates are desirable to decrease the time of the altitude estimation convergence. In addition a parametric study on the EKF estimation performance must be carried out varying the sensor parameters and noise.

References

[1] Flight Safety Foundation "ASN Aircraft accident McDonnell Douglas DC-9-21 LN-RLM Oslo-Fornebu Airport (FBU)," Nov. 7 2018. [Online]. Available: https://aviation-safety.net/database/record.php?id=19730130-1. [Accessed Nov. 7, 2018].

[2] National Transportation Safety Board Accident Report, Nov. 7 2018. [Online]. Available: https://www.ntsb.gov/investigations/AccidentReports/Pages/AAR7513.aspxNTSB/AAR-75-13. [Accessed Nov. 7, 2018].

[3] Flight Safety Foundation, [Online]. Available: https://aviation-safety.net/database/record.php?id=19840728-0 Soviet Transports Boureau. [Accessed Nov. 7, 2018].

[4] Flight Safety Foundation, [Online]. Available: https://reports.aviation-safety.net/1994/19940302-0_MD82_N18835.pdf. [Accessed Nov. 7, 2018].

[5] Flight Safety Foundation, [Online]. Available: https://flightsafety.org/ap/ap_july99.pdf. [Accessed Nov. 7, 2018].

[6] National Transportation Safety Board Accident Report, [Online]. Available: https://www.ntsb.gov/_layouts/ntsb.recsearch/Recommendation.aspx?Rec=A-96-141

[7] Flight Safety Foundation, [Online]. Available: https://aviation-safety.net/database/record.php?id=19971010-0&lang=es

[8] Flight Safety Foundation, [Online]. Available: http://aviation-safety.net/database/record.php?id=19990407-0&lang=es

[9] Flight Safety Foundation, [Online]. Available: http://aviation-safety.net/database/record.php?id=19991017-0&lang=es. [Accessed Nov. 7, 2018].

[10] National Transportation Safety Board Accident Report, [Online]. Available: http://www.ntsb.gov/aviationquery/brief2.aspx?ev_id=20060618X00757&ntsbno=NYC06FA138&akey=1. [Accessed Nov. 7, 2018].

[11] Flight Safety Foundation, [Online]. Available: http://flightsafety.org/asw/sept10/asw_sept10.pdf. [Accessed Nov. 7, 2018].

[12] National Transportation Safety Board Accident Report. [Online]. Avaliable: https://www.ntsb.gov/_layouts/ntsb.recsearch/Recommendation.aspx?Rec=A-96-015

[13] "Faulty speed indicators suspected as cause of Russian plane crash." The Guardian News Paper. February 14, 2018. [Online]. Avaliable: https://www.theguardian.com/world/2018/feb/13/faulty-speed-indicators-suspected-as-cause-of-russian-plane-crash. [Accessed Nov. 7, 2018].

[14] Flight Safety Foundation, Nov. 7 2018. [Online]. Available: https://aviation-safety.net/database/record.php?id=19961002-0. [Accessed Nov. 7, 2018].

[15] D. Koening. "Officials consider role of speed readings in Lion Air crash", MSN News. November 6, 2018. [Online]. Avaliable: https://www.msn.com/en-au/news/world/officials-consider-role-of-speed-readings-in-lion-air-crash/ar-BBPoiMy?ocid=spartandhp. [Accessed Nov. 7, 2018].

[16] Barthe, J. "Unreliable Speed," Safety First - The Airbus Safety Magazine, Number 5, December 2007.

[17] EASA Equivalent Safety Finding ESF F-69. [Online]. Avaliable: https://www.easa.europa.eu/sites/default/files/dfu/ESF%20F-69%20Consultation.pdf

[18] Australian Transport Safety Bureau. [Online]. Available: https://www.atsb.gov.au/media/5773029/ao-2015-149-final.pdf

[19] S. Gururajan, M. L. Fravolini, M. Rhudy, A. Moschitta, and M. Napolitano, "Evaluation of sensor failure detection, identification and accommodation (SFDIA) performance following common-mode failures of pitot tubes," SAE 2014 Aerospace Systems and Technology Conference, No. 2014-01-2164, September, 2014.
[20] M. L. Fravolini, G. Del Core, U. Papa, P. Valigi, and M. R. Napolitano, "Data-Driven Schemes for Robust Fault Detection of Air Data System Sensors," IEEE Trans. Control Syst. Technol., vol. 27, no. 1, pp. 234–248, 2019.
[21] Stevens, B. Lewis, F. Johnson, E. "*Aircraft Control and Simulation,*" John Wiley & Sons, NY, 2016.
[22] Napolitano, M. R. "*Aircraft Dynamics: from Modeling to Simulation,*" John Wiley & Sons, Hoboken, NJ, Nov 2011.
[23] M.R. Napolitano, S. Cascianelli, S. Gururajan, M.B. Rhudy, M.L. Fravolini, "Experimental Evaluation of Two Pitot Free Analytical Redundancy Techniques for the Estimation of the Airspeed of an UAV," SAE Int. J. Aerosp. 7(1):2014.Napolitano, M.R. Rhudy, M. Chao, H. Fravolini, M. Gururajan, S. "Performance Evaluation of Neural Network Based Approches for Airspeed Sensor Failure Accomodation on a Small UAV," 21st Mediterranean Conference on Control & Automation (MED), 25-28 June 2013.
[24] M.R. Napolitano, M.B. Rhudy, H. Chao, M.L. Fravolini, S. Gururajan, "Performance Evaluation of Neural Network Based Approches for Airspeed Sensor Failure Accomodation on a Small UAV," 21st Mediterranean Conference on Control & Automation (MED), 25-28 June 2013.
[25] Saed Hussain, Maizura Mokhtar, Joe M. Howe, "Sensor Failure Detection Identification and Accommodation Using Fully Connected Cascade Neural Network", Industrial Electronics IEEE Transactions on, vol. 62, pp. 1683-1692, 2015, ISSN 0278-0046.
[26] Balzano, F. Fravolini, M.L. Napolitano, M.R. d'Urso, S. Crispoltoni, M. del Core, G. "Fault Detection With An Augmented Floating Limiter", IJAE - International Journal of Aerospace Engineering, 2018
[27] F. Balzano, M.L. Fravolini, M.R. Napolitano, S. d'Urso, M. Crispoltoni, G. del Core, "Fault Detection With An Augmented Floating Limiter", International Journal of Aerospace Engineering, 2018.
[28] S. Gururajan, M.B Rhudy, M.L. Fravolini, H. Chao, M.R. Napolitano, "Failure detection and accomodation approaches for the airspeed sensor on a small UAV", Fault Detection: Classification, Techniques and Role in Industrial Systems. UK Edition, Nova Science Pub Inc; December 31, 2013.
[29] Seckel, E. M. J. J. (1971), "The stability derivatives of the Navion aircraft estimated by various methods and derived from flight test data" (FAA-RD-7106), Technical report, Department of Transportation, Federal Aviation Administration.
[30] Oh, S.M., Johnson E. "Development of UAV Navigation System Based on Unscented Kalman Filter", AIAA Guidance, Navigation, and Control Conference and Exhibit, August 2006, Keystone, Colorado.